MAGNETRON SPUTTERED ZNO ON MWCNT FOR LI-ION BATTERY NEGATIVE ELECTRODES

H. Akbulut, T. Cetinkaya, M. O. Guler, M. Uysal

Sakarya University, Engineering Faculty, Department of Metallurgical & Materials Engineering, Esentepe Campus, 54187, Sakarya/TURKEY, e-mail: akbulut@sakarya.edu.tr

Abstract

In this study, ZnO/MWCNT) nanocomposites are produced by magnetron sputtering radio frequency (RF) plasma process as anode materials for Li-ion batteries. The physical, structural, and electrochemical behaviors of the nanocomposite electrodes in the form of ZnO shell on the MWCNT core are discussed. The thickness of the ZnO shell is controlled by changing plasma power at the constant deposition time of 5 min. and the shell thickness effect is investigated on the structural and electrochemical properties. The greatly enhanced electrochemical performance is mainly due to the morphological stability and reduced diffusion resistance, which are induced by MWCNT core and deposited ZnO shell. The outstanding long-term cycling stability and rate capability is a result excellent reinforcement effect of the MECNTs and functionally gradient material (FGM) structure. The nanoscale ZnO/MWCNT network provides good electrical conductivity, and the creation of open spaces that buffer a large volume change during the Li-alloying/de-alloying reaction.

Keywords: Lithium-ion batteries, ZnO/CNT nanocomposite, core-shell structure, rate capability, energy storage

1. INTRODUCTION

Recently, lithium ion batteries are receiving considerable attention over other rechargeable cells in portable electronic devices. Several researches has been done in increasing the energy density of cells by improving the quality of cathode and anode electrode materials. The ideal anode material for lithium-ion battery should have high lithium storage capability and very stable structure for long cycleabilty [1]. Energy demand and storage with green source is becoming an utmost important topic in the last decades. Nowadays, Li-ion batteries are employed as power source for daily-used devices and research is currently yielding a stream of improvements to traditional Li-ion battery technology, focusing on energy density, durability, cost, and intrinsic safety [2]. Energy storage systems including supercapacitors and lithium ion batteries typically appear in a rigid plate, which is unfavorable for many applications, especially in the fields of portable and highly integrated equipments, which require small size, lightweight, and high flexibility [3].

In particular, microbatteries could play a considerable role in the next future Li-ion battery market due to the high demand of on board power supplies for smart technologies, such as smart medicine and implantable medical tools, micro-electromechanical systems (MEMS) and for many others autonomous devices [4, 5]. These several emerging microtechnology branches, such as microelectromechanical system (MEMS) devices and small-scale medical devices, require portable power supplies with a very small dimension [6, 7]. Vacuum evaporation techniques are reported to be efficient and flexible methods for producing ZnO based oxide nano structured films and materials for microbatteries [8]. In the microbattery producing techniques, cathode and anode electrodes can be directly deposited from metallic and oxide substrates to control the porosity level, film thickness, electrode dimensions and physical properties [9-12].

Zinc based materials, Zn and ZnO, are the promising candidates for Li–M-MO alloy anode materials. They can alloy with Li, has various intermetallic phases, and displays a low operating voltage. Additionally, Zn and ZnO are abundant, cheap, and environmentally benign materials. Considering these merits, Zn and ZnO may be a highly appropriate element for use as the anode in Li-ion batteries [13]. ZnO especially is an

attractive material as a potential substitute for the conventional graphite anode in lithium-ion batteries, because the theoretical capacity of ZnO (978 $mAhg^{-1}$) has been estimated to be superior to that of graphite (372 mAh g^{-1}) but also owing to the reasonably low potentials and high volumetric and gravimetric capacities [14].

Although Zn and ZnO have many merits as a Li-ion battery anode material, only a few studies have been reported. Therefore, the practical use of ZnO powders as a negative electrode for lithium-ion batteries is still hindered by several major problems: poor cycleability, resulting from the severe volume expansion and contraction during the alloying-dealloying cycles with Li^+ ions and the associated charge transfer process, and the pulverization and the agglomeration of primitive particles, which drastically reduces the total entrance/exit sites available for Li^+ ions [15]. On the other hand, the poor electronic conductivity hinders the reaction with lithium during the first discharge.

To prevent the electrode pulverization and therefore, electrochemical energy capacity fading, producing nanocomposite electrodes seems to be a solution. Carbon nanotube based papers or so-called "Buckypapers" that contains high concentrations of carbon nanotubes have the potential to form strong and lightweight composite materials. Many different CNT composites with a variety of Li storage materials have been studied for use as anode materials, such as Zn, Sn, Sb, ZnO, TiO_2 and SnO_2, easily develop cracks during the charge–discharge process in spite of their significantly high electrochemical Li intercalation capacities. The breakdown of the electrode is a major cause of rapid degradation of their capacities as a consequence of the large specific volume change during the lithiation and de-lithiation reactions. The combining of MWCNTs that can hinder the agglomeration and enhance the electronic conductivity of the active materials is responsible for the enhanced cyclic performance [16-19].

However, despite the possible uses of ZnO in Li-ion batteries, the electrochemical behavior and the mechanism of the reaction between ZnO and Li have not been investigated in detail for the thin film ZnO on the MWCNT surfaces produced by vacuum vaporization technique of RF sputtering. In this study, the electrochemical behavior and the structure of ZnO/MWCNT electrode for Li-ion thin film microbatteries were investigated. ZnO active materials in the nanocrystalline state were coated on the highly porous MWCNT buckypapers in the form of core-shell structure via RF plasma sputtering technique directly from ZnO substrates.

2. EXPERIMENTAL DETAILS

The MWCNTs over 80.0 μm in length with the outer diameter of 50 nm were used as stress buffering and conductive network in this study supplied by Arry International (Germany). The nanotubes were synthesized by catalytic carbon vapour deposition (CCVD). According to the provider specifications, purities of the MWCNTs are all more than 95 %, and contents of impurities (metal catalyst, amorphous carbon and ash) are all less than 5 wt. %. Chemical oxidation of MWCNTs was carried out with a mixture of H_2SO_4 (sulfuric acid) and HNO_3 (nitric acid) acids in ratio 3:1 for 3 h after annealing and treating in HCl (hydrochloric acid) for impurity removing. The oxidized MWCNTs were first dispersed into water by the aid of SDS (sodium dodecyl sulfate) surfactant and sonicated to form a well dispersed suspension which subsequently was vacuum filtered through PVDF (polyvinylidene fluoride) membrane filters of 220 nm pore size to form buckypapers. The optimization route of the MWCNT buckypaper production can be found in our previous work [19]. In each experiment, a MWCNT suspension at a concentration of 1mg/ml was prepared by tip sonication for 60 min. Then the resulting solid was washed up, and the sample dried in the vacuum at 40°C for overnight, and the MWCNT films were peeled-off from the filtration membrane. The average thickness of the produced buckypapers is approximately 80 □m and their diameter about 16 mm.

The coating of ZnO on the MWCNT surfaces have been performed in a multifunctional magnetron sputtering PVD unit equipped with thermal evaporation, D.C. and R.F. units. Deposition of thin layer ZnO on the MWCNTs has been carried out using high-purity ZnO (99.99 % purity) target by R.F. magnetron sputtering. Before starting the coating process, the chamber was evacuated into 10^{-4} Pa by a turbo molecular pump and

then back filled with argon up to 1.0 Pa pressure. The substrates were not deliberately heated or cooled during R.F. plasma. The coating time was considered to produce a shell layer with a thickness between 10-15 nm on the single MWCNT surfaces. Therefore, the magnetron sputtering powers were chosen as 75 W, 100 W and 125 W and the total deposition time of 5 min. The R.F. magnetron sputtering from ZnO target was carried out at high-purity oxygen (99.999 %) and argon (99.9999 %) gas mixture by using 90 % argon and 10 % oxygen gas mixture atmospheres. Buckypapers were weighed out by using an ultra-microbalance (Radwag UYA 3Y) in order to determine the amount of ZnO on the surfaces of buckypapers before and after deposition processes. The gases were introduced through individual needle valves after the vacuum chamber was evacuated to about 10^{-4} Pa by a turbo molecular pump.

The surface and cross-section morphologies of the produced buckypapers and ZnO coated buckypaper electrodes were observed by field emission scanning electron microscopy (FESEM-Philips XL 30SFEG).. The phase structures of the MWCNT buckypapers and deposited films were investigated by X-ray diffraction (XRD) (Rigaku D/MAX 2000 with thin film attachment) with CuK□ radiation. The grain size of the thin films was calculated by using the Scherrer's formula and rechecked by Williamson-Hall equation.

Coin type CR2016 cells were assembled in an argon-filled glove box. The electrolyte solution was 1 M $LiPF_6$ in EC/DMC (1:1 by volume). The electrochemical performance of the ZnO/MWCNT nanocomposites was evaluated by galvanostatic discharge–charge measurement using a computer-controlled battery tester between 0.02 and 2.5 V. The cells were cyclically tested on a MTI Model BST8-MA electrochemical analyzer using 1C current density over a voltage range of 0.02–2.5 V. All the potentials indicated here were referred to the Li/Li^+ electrode potential. All electrochemistry tests were carried out at room temperature (25 °C).

3. RESULTS & DISCUSSIONS

3.1 Morphological observations

The buckypapers were successfully produced from chemically oxidized MWCNTs as flexible, uniform, smooth, and crack-free disks and easily peeled-off from PVDF membrane. Effects of oxidants on formation of MWCNT buckypaper were studied in our previous work and H_2SO_4 and HNO_3 acids in the ratio 3:1 was found most suitable for our purposes to produce MWCNT network skeleton supported electrodes [20] The picture showing flexibility and the FESEM surface image of the buckypaper are shown in Fig. 1. The buckypaper sheet (Fig. 1a) shows a great number of long, curled and randomly oriented MWCNT bundles, with diameters ranging between 40 and 70 nm. Porous structure that appropriate for composite manufacturing was obtained as shown in Fig. 1b.

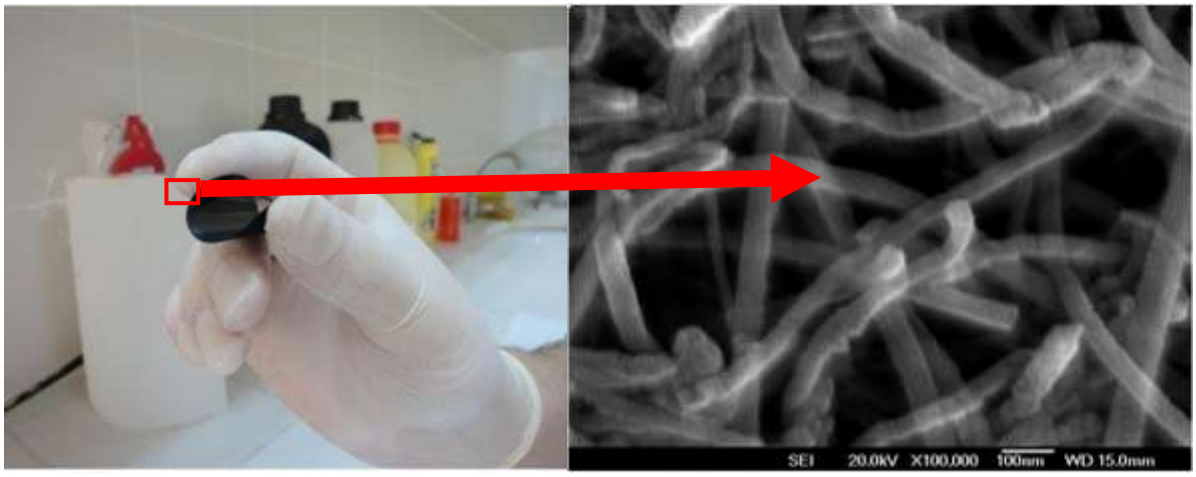

Figure 1. a) Flexible free-standing MWCNT buckypaper and b) FESEM image of buckypaper.

Fig. 2 reveals typical FESEM of MWCNT buckypapers coated with ZnO nanoparticles at different RF plasma powers. The FESEM morphologies of ZnO/MWCNT nanocomposites produced at various RF plasma powers, including 75 W, 100 W and 125 W are presented in Fig. 2a, 2b and 2c show very fine ZnO nanoparticles and particle size increment with increasing RF plasma power. The coated MWCNT in the buckypapers exhibit relatively uniform diameter and length with a high aspect ratio. Increasing RF plasma power resulted in thicker ZnO phase on the MWCNT surfaces. The calculation of ZnO thickness with weight measurement before and after RF plasma coating revealed that the coating thickness around the MWCNTs are between 10 and 15 nm .Fig. 2c presents FESEM images of ZnO/MWCNT nanocomposite at higher magnification showing very well attached ZnO on the MWCNT surfaces. As seen from the TEM image in Fig 2d, ZnO was deposited around the MWCNTs forming a core-shell structure. Since the RF plasma treatment of MWCNTs also creates defects on the sp^2 bonds, it is an expected phenomenon of nucleation and growth of ZnO on the MWCNT phase. As can be seen from the FESEM micrographs in the Fig. 2,

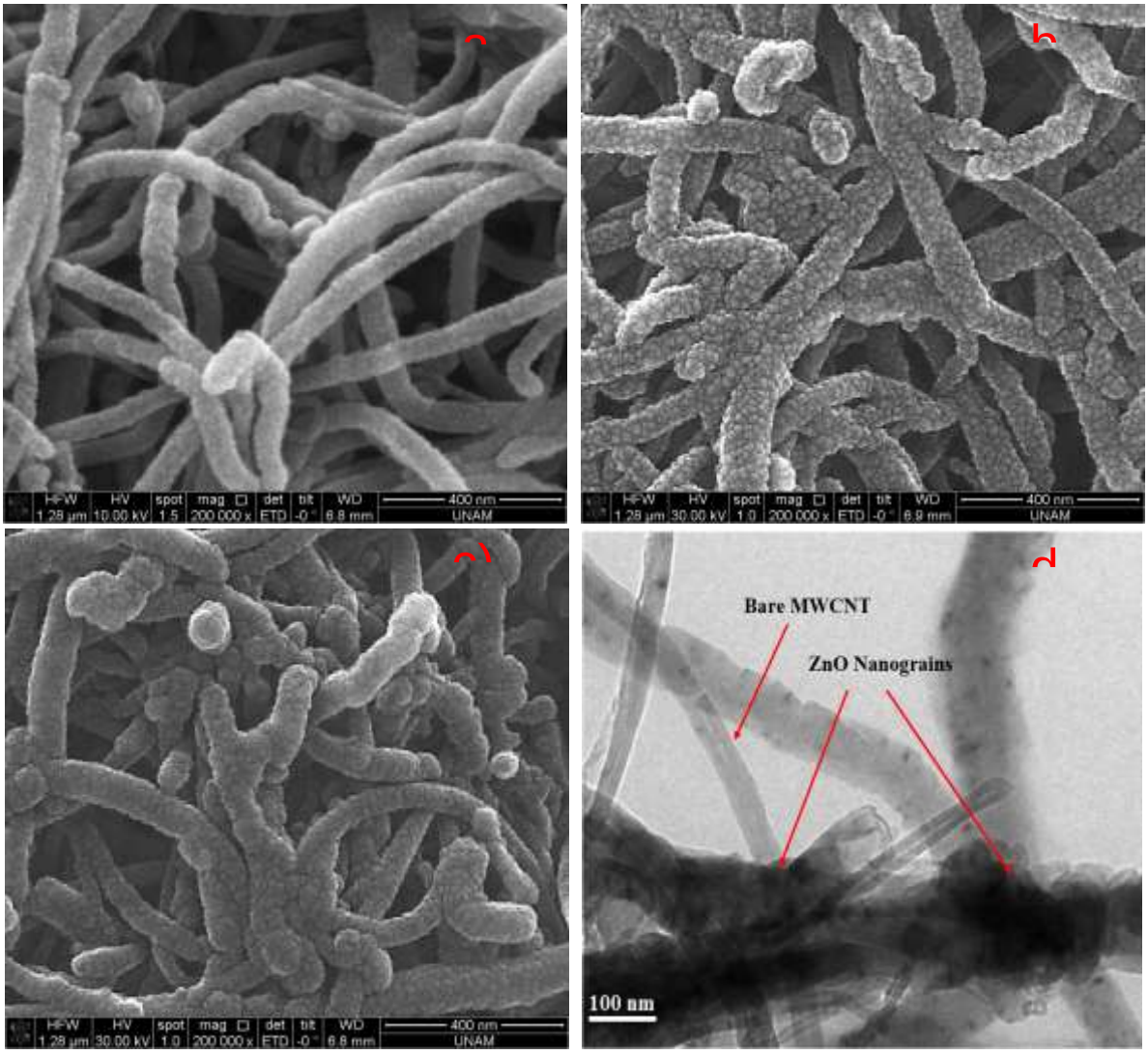

Figure 2. FESEM images of the films produced on the MWCNTs under different RF plasma powers; a) 75 W, b) 100 W, c) 125 W and d) TEM images of ZnO/MWCNT nanocomposite structure showing core-shell structure.

ZnO is formed on the surfaces with very fine nano grains, which expected to accelerate Li diffusion. Moreover, surface EDS dot-mapping analyze of the ZnO/MWCNT nanocomposite electrode demonstrates homogenous distribution of the ZnO nanograins on the surface of MWCNT buckypaper (Fig. 3). XRD

patterns for the as-produced buckypaper and ZnO thin films deposited under various oplasma powers are depicted in Fig. 4. All reflexes were assigned to carbon (JCPDS 026-1080) and hexagonal zinc oxide (JCPDS-36-1451). As the plasma power increases, the intensity of ZnO (002) and (111) peaks increase remarkably. Higher plasma power provides more energy to enhance mobility of the deposition atoms, which improves the crystal quality of the films. Furthermore, increasing plasma power resulted decreasing intensity of the MWCNT buckypaper due to increasing thicknes of the ZnO layer on the surface of MWCNT buckypaper. The preferred texture orientations were also shown a change by increasing the RF plasma power. Increase in the RF plasma power leads to alter of the texture in the deposited zinc oxide films. Lattice parameters of the deposited thin films were calculated and "c" parameter was found to be 5.204 Å, 5.208 Å and 5.212 Å, and "a" parameter was found to be 3.191 Å, 3.189 Å and 3.184 Å for the films deposited under 75 W, 100 W and 125 W RF powers, respectively. The hexagonal wurtzite ZnO crystal structure shown in Fig 5. When the calculated values compared with the standard "c" and "a", values obtained from JCPDS 36-1451, it was found that an increase in the "c" parameter (c=5.206 Å according to JCPDS 36-1451) and a decrease in the "a" parameter (a=3.249 Å according to JCPDS 36-1451). Such a behavior has been observed for ZnO films and has been attributed to the possible presence of a significant number of oxygen vacancies leading to a reduction of interatomic distances, i.e., a reduction in parameter “a”, and increase in space between the layers, which corresponds with an increase in “c” [21-22].

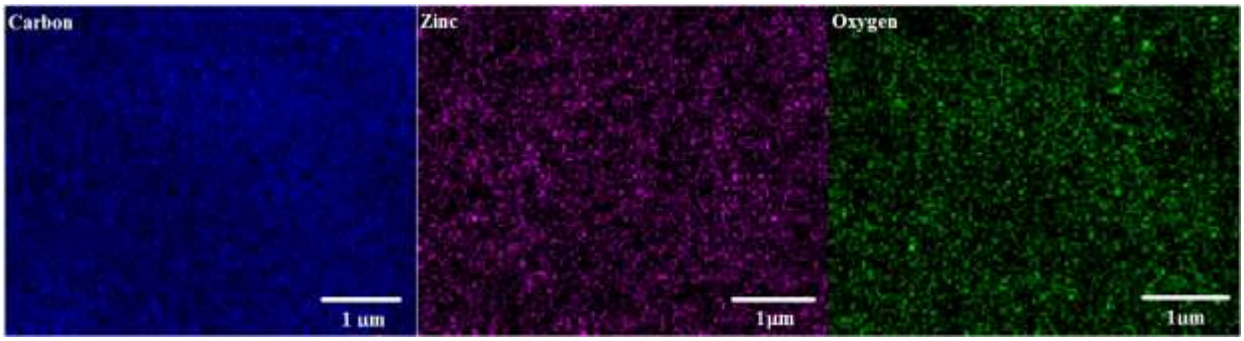

Figure 3. Surface EDS dot-mapping of ZnO/MWCNT nanocomposite electrode.

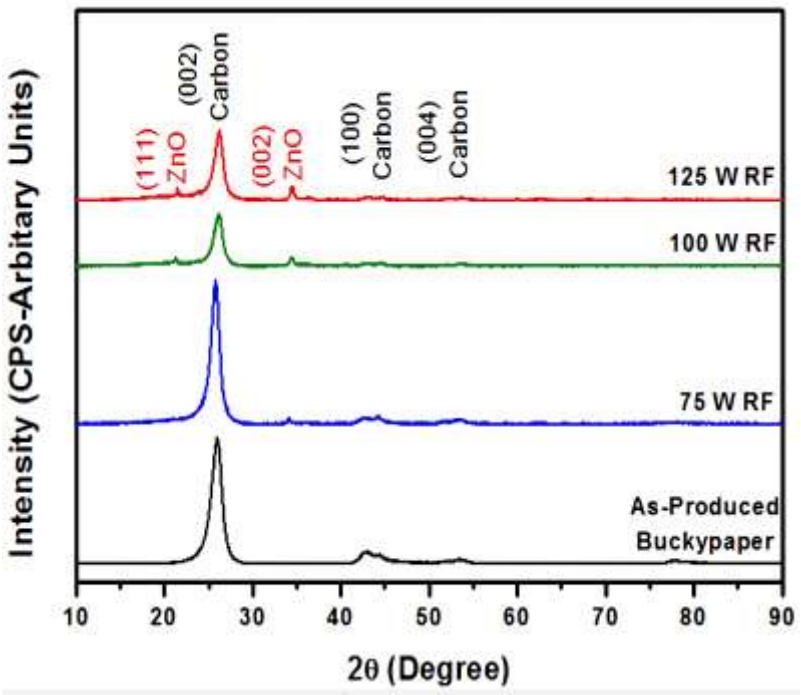

Figure 4. XRD patterns of bare buckypaper and ZnO/MWCNT nanocomposites deposited at various RF powers.

The mean grain sizes of the deposited ZnO thin films were calculated via Scherrer's formula and shown in Fig. 6. The grain size of the ZnO was also calculated with Williamson-Hall method and the results showed a little bit smaller grain sizes by Williamson Hall (only 3-5 %). The grain sizes of the films are found to increase with the increase in the RF plasma power, which clearly reveals the improvement in the crystallinity. The calculated values are 4.78 nm, 8.56 and 12.38 nm for the films deposited at 75 W, 100 W and 125 W powers, respectively. Under the condition of high plasma power, the species ejected from the target surface would suffer from higher temperatyures besause of high collision between the plasma gases and evaporated species. Accordingly, vapor species could be growth also laterally. Hence, the mean grain sizes of the films were increased with increasing plasma power.

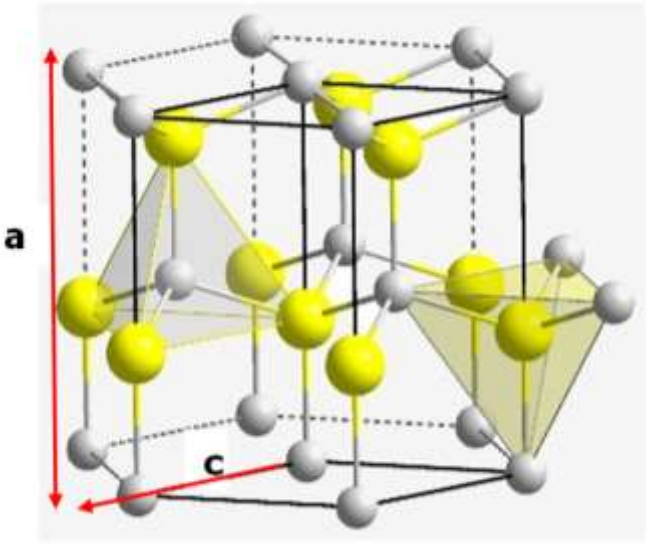

Figure 5. The hexagonal wurtzite ZnO crystal structure.

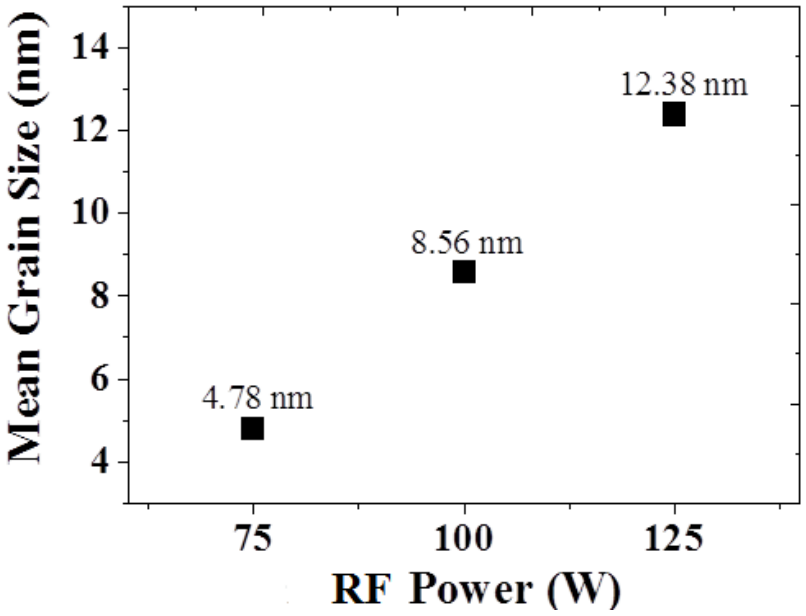

Figure 6. Mean grain sizes of the ZnO films deposited at various RF plasma powers.

3.2 Electrochemical Results

The galvanostatic discharge–charge curves at current density 12 $mAdm^{-2}$ (1C) of MWCNT/ZnO MWCNT/ZnO anode electrodes between 0.2 and 2.5 V vs. Li^+/Li is presented in Fig. 7. There are two plateaus between 1.2-1.6 V and 0.65-0.8 V referring alloying/dealloying reactions. The, two majors cathodic peaks around 0.35 V and 0.75 V were observed in the galvanostatic profiles, which can be assigned to the reduction of ZnO into Zn and the formation of lithium–zinc alloy, and the decomposition of electrolyte and hence the growth of an organic-like-layer [23]. The discharge capacities and the capacity fade values for the first and last three cycles are listed in Table 1 and Table 2.

The discharge capacity of the ZnO/MWCNT decreases to 731 $mAhg^{-1}$, 554 $mAhg^{-1}$ and 500 $mAhg^{-1}$ in the second cycle and 728 $mAhg^{-1}$, 553 $mAhg^{-1}$ and 498 $mAhg^{-1}$ in the third cycle for the films deposited at 75 W, 100 W and 125 W, respectively. The capacity fade is recorded to be lower (21 % at the third cycle) in the nanocomposite electrode that produced at 75 W RF power and fading is slower in comparison with the electrodes deposited at 100 W and 125 W. As can be seen from the Table 2, the capacity fading is very slow with increasing cycle number, especially for the electrode deposited at 75 W, and at the 100th cycle the electrode shows nearly stable discharge capacity. At the end of the 100th cycle, the electrode exhibits a discharge capacity of 661 $mAhg^{-1}$ and a capacity fade of 32 %. It is well known that CNT shows the reaction with li-ions. Therefore, it is possible that there is a discharge capacity contribution of the ZnO/MWCNT composites. However, it is reported that MWCNT buckypaper demonstrates 74 $mAhg^{-1}$ discharge capacity in previous work [24]. In this study, although the surface of the MWCNTs were coated with ZNO nanograins, it is believed that the discharge capacity contribution of the buckypaper less than 75 $mAhg^{-1}$. For this reason, the discharge capacity contribution of the MWCNT was tolerated in this study. It is known that cycling performance of metal oxide based anodes is significantly affected by the volume-change of active particles during lithium insertion–extraction process. If active particles could not tolerate the volume-change, they will pulverize into smaller particles, and electrode is strongly polarized as a result. Therefore, the ZnO/MWCNT/ nanocomposite electrodes combine the advantages of nanomaterials and the volume-change tolerance of microspheres, which is extremely favorable to lithium insertion and extraction.

Table.1. The galvanostatic discharge capacity changing of the nanocomposite electrodes for the initial third cycles.

RF Power (W)	1st Cycle (mAh/g)	2nd Cycle (mAh/g)	3rd Cycle (mAh/g)	Capacity Fade (%)
75	979	783	775	21
100	881	554	553	38
125	793	500	498	38

Table.2. The galvanostatic discharge capacity changing of the nanocomposite electrodes for the last third cycles.

RF Power (W)	50th Cycle (mAh/g)	80th Cycle (mAh/g)	100th Cycle (mAh/g)	Total Capacity Fade (%)
75	666	663	661	32
100	493	489	487	45
125	444	435	427	46

Fig. 8 shows the cycling performance and the coulombic efficiencies of the nanocomposites deposited at different plasma powers. As seen from the Fig.8a, The discharge capacities of the nanocomposite electrodes

become nearly stable after 30-35th cycling. Decreasing the RF power reveals better capacity fading. The coulombic efficiencies are seen very high after 10th cycle and very close to 100 %. The faster capacity fading for the films oxidized at 100 and 125 W RF powers may be attributed to the intrinsic structure instability during lithium insertion/extraction and the aggregation of nanoparticles. It is believed that the incorporation of MWCNT buckypapers improved the Li electro activity of the ZnO nanoparticles because of their beneficial effect on the conductivity, efficient electron paths, and aggregation control of active nanoparticles.

Further we investigated the rate performance at various currents starting from 20/C to 4Cfor the three electrodes of 5 cycle each (Fig. 9). Fig. 9 shows the rate performance of for the electrodes produced by using 100 W, 125 W and 125 W RF powers. The discharge capacities of anode electrodes produced by using 75 W, 100 W and 125 W RF powers remain 822 $mAhg^{-1}$, 710 $mAhg^{-1}$, and 635 $mAhg^{-1}$ after 5 cycles at a current density of “C/20”. As normally expected, the discharge capacities are decreased with increasing charging rate. The reduction in capacity for the increase of current rate can be explained as due to the increasing interface resistance between (i) electrolyte and active materials at a high current rate (ii) active material and current collector [25]. Increasing the charging rate beyond 1C the discharge capacities of all the electrodes are decreased between 10-15 %. After charging at the 4C condition the cells were retuned to be discharged at 1C again after 25th cycle. A remarkable increase is seen in the discharge capacities for all the nanocomposite electrodes. The new discharge capacities at the 30th cycle were found as 562 $mAhg^{-1}$, 402 $mAhg^{-1}$ and 335 $mAhg^{-1}$ for the nanocomposites deposited at 75 W, 100 W and 125 W, respectively were obtained after 30 cycles

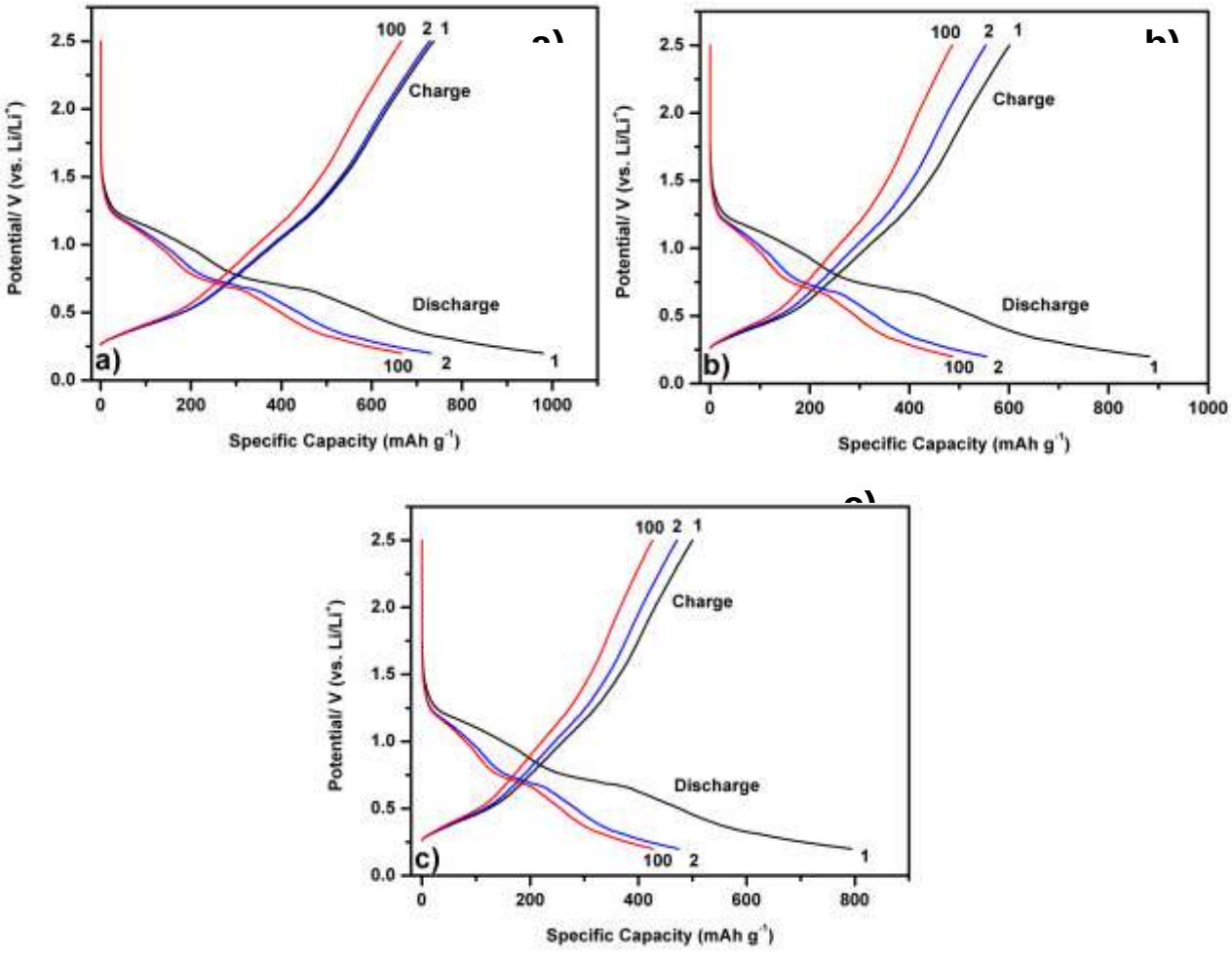

Figure 7. Galvanostatic charge-discharge curves of the films deposited at different RF powers; a) 75 W, b) 100 W and c) 125 W.

In the nanocomposite produced at 75 W RF power recovered its capacity approximately more than 85 % even at increased number of the cycle condition. Such behavior indicates that the excellent rate capacity retention can be attributed to the formation of high efficient Li^+ transportation pathways in the 3D conductive network and also unique reinforcing effect of the MWCNTs that provide not only load transfer from the active matrix ZnO, but also exhibit functionally gradient material (FGM) structure. Because of the thin film coating and a thinner core-shell structure in the nanocomposite produced at 75 W RF power the residual stresses arisen from volume increase during charging/discharging cycles are buffered with stress relaxation mechanisms.

The residual stresses are expected to be relaxed both in the radial direction of the produced buckypaper and also through the center of the buckypaper because of the FGM structure. The stress relaxation in our buckypaper electrode is modeled in the Fig. 10. It can be concluded in this study that the reason of so high retained electrochemical performance in the metal oxide/MWCNT nanocomposites is the compact and stout wall of the MWCNTs accommodates large volume expansion, cushioning against the large internal stresses caused by tin aggregation during charge/discharge cycles and allowing excellent cycle duration by preventing electrode pulverization [26, 27].

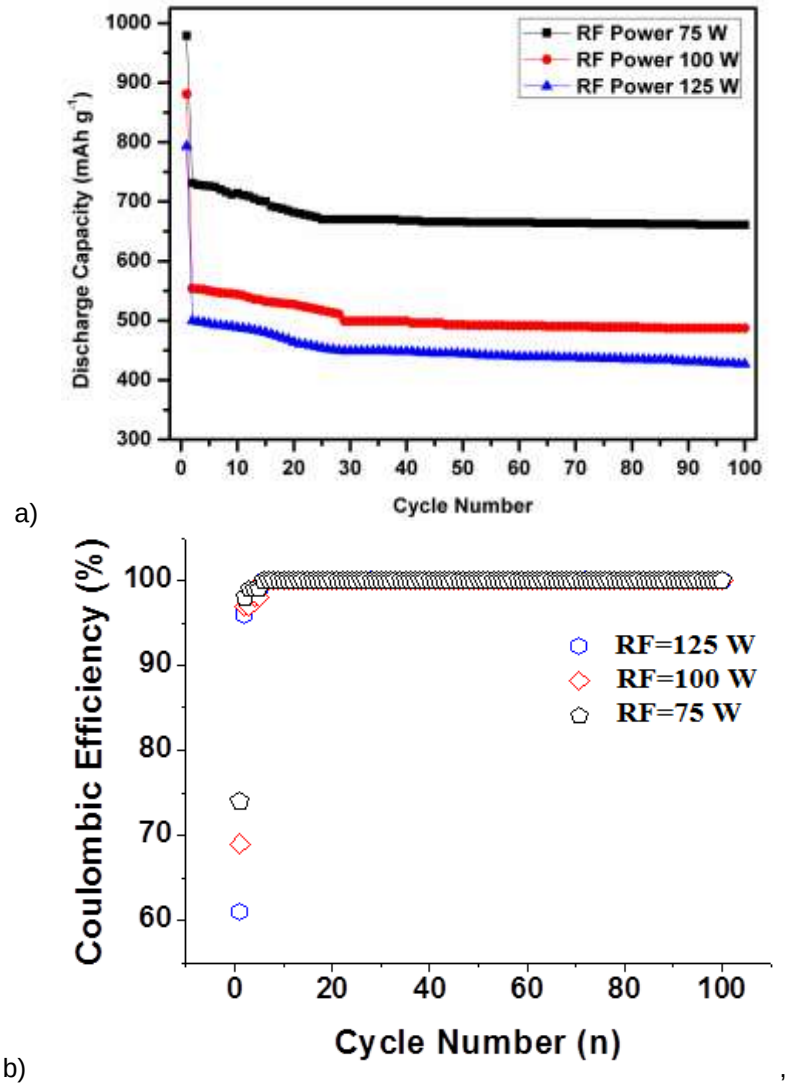

Figure 8. a) Discharge capacity – cycle diagram for the nanocomposite electrodes deposited under different plasma powers and b) Coulombic efficiencies of the electrodes.

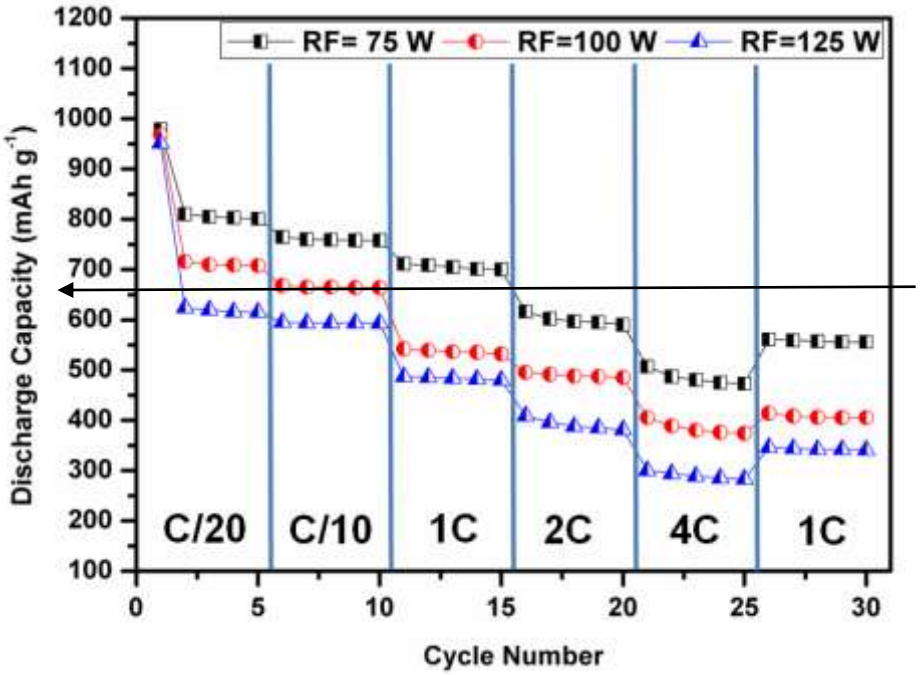

Fig. 9. Rate performance of the electrodes produced by using 75 W, 100 W and 125 W RF powers.

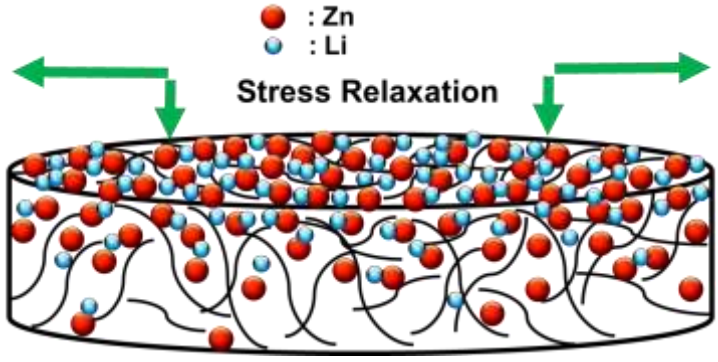

Fig. 10. Stress relaxation mechanism in the nanocomposğte electrodes due to MWCNT reinforcedment and FGM structure

CONCLUSIONS

ZnO nanocrystals were coated on the MWCNT buckypapers developed using the vacuum filtration process. ZnO thin films were prepared on buckypaper substrates via RF plasma sputtering. The highly uniform ZnO nanocrystals with crystal size between 4.78 and 12.38 nm were uniformly deposited on the surface of MWCNT based buckypapers. As anode material for Li-ion battery, the nanocomposites revealed superior cycling stabilities up to 100 cycles with a capacity of 661 $mAhg^{-1}$. Such good stability was ascribed to the strong adhesion of ZnO nanocrystals on the MWCNT support, which has high electronic conductivity and possesses excellent stress relaxation with good flexibility. The stress relaxation provided by excellent load bearing ability and FGM structure was assessed to be another unique mechanism that provides very high capacities and stability. The experimental investigation and results in this work showed that ZnO/MWCNTs nanocomposites produced by RF plasma sputtering can be good candidates for Li-ion microbaterries if the shell thickness and the penetration depth of the active ZnO are controlled by RF plasma parameters.

ACKNOWLEDGEMENTS

This work was supported by the Scientific and Technological Research Council- of Turkey (TUBITAK), under the contract number 109M464. The authors thank the TUBITAK MAG workers for their financial support.

REFERENCES

[1] Thomas, R., Rao, K.Y., Rao, G.M. Morphology and electrochemical performance of graphene nanosheet array for Li-ion thin film battery. *Electrochimica Acta*, 2013, 108, 458.

[2] Park, C.M., Kim, J.H., Kim, H., Sohn, H.J. Li-alloy based anode materials for Li secondary batteries. *Chemical Sociaty Review*, 2010, 39, 3115.

[3] Ren, J., Li, L., Chen, C., Chen, X., Cai, Z., Qiu, L., Wang, Y., Zhu, X., Peng, H. Batteries: Twisting Carbon Nanotube Fibers for Both Wire-Shaped Micro-Supercapacitor and Micro-Battery. *Advenced Materials*, 2013, 25, 1224.

[4] Golodnitsky, D., Nathan, M., Yufit, V., Strauss, E., Freedman, K., Burstein, L., Gladkich, A., Peled, E. Progress in three-dimensional (3D) Li-ion microbatteries. *Solid State Ionics*, 2006, 177, 2811–2819.

[5] Lamberti, A., Garino, N., Sacco, A., Bianco, S., Manfredi, D., Gerbaldi, C. Vertically aligned TiO_2 nanotube array for high rate Li-based micro-battery anodes with improved durability. *Electrochimica Acta*, 2013, 102, 233.

[6] Zadin, V., Brandell, D., Kasemägi, H., Lellep, J., Aabloo, A. Designing the 3D-microbattery geometry using the level-set method. *Journal Power Sources*, 2013, 244, 417.

[7] Yue, C., Yu, Y., Yin, J., Wong, T., Zang, Y., Li, J., Kanga, J. Fabrication of 3D hexagonal bottle-like Si–SnO_2 core–shell nanorod arrays as anode material in on chip micro-lithium-ion-batteries. *Journal of Materials Chemistry A*, 2013, 1, 7896.

[8] Zhang, L., Peng, G., Yang, X., Zhang, P. High performance $LiFePO_4$/C cathode for lithium ion battery prepared under vacuum conditions. *Vacuum*, 2010, 84, 1319.

[9] Chiu, K.F., Chen, C.C., Lin, K.M., Lin, H.C., Lo, C.C., Ho, W.H., Jiang, C.S. Modification of sputter deposited solid-state electrolyte thin films. *Vacuum,* 2010*,* 84, 1296.

[10] Kavanoz, H.B., Yağci, O., Yalçın, Z., İçelli, O., Altındal, A., Okutan, M., Mann, K.S. Photon parameters for γ-rays sensing properties of some thick oxide films. *Vacuum*, 2013, 101, 238.

[11] Mohameda, S.H., Venkataraj, S. Thermal stability of amorphous molybdenum trioxide films prepared at different oxygen partial pressures by reactive DC magnetron sputtering. *Vacuum*, 2007, 81, 636.

[12] Guler, M.O., Cevher, O., Cetinkaya, T., Tocoglu U., Akbulut, H. Nanocomposite anodes for lithium-ion batteries based on Sno2 on multiwalled carbon nanotubes*. International Journal of Energy Research*, 2014, 38, 487.

[13] Hwa, Y., Sung, J.H., Wang, B., Park, C.M., Sohn, H.J. Nanostructured Zn-based composite anodes for rechargeable Li-ion batteries. *Journal of Materials Chemistry*, 2012, 22, 12767.

[14] Belliard, F., Connor, P.A., Irvine, J.T.S. Novel tin oxide-based anodes for Li-ion batteries. *Solid State Ionics*, 2000, 135, 163.

[15] Belliard, F., Connor, P.A., Irvine, J.T.S. Doped tin oxides as potential lithium ion battery negative electrodes. *Ionics*, 1999, 5, 450.

[16] Li, Y.N., Yang, J., Jiang, M., Synthesis and characterization of Sb/CNT and Bi/CNT composites as anode materials for lithium-ion batteries. *Material Letters*, 2008, 62, 2092.

[17] Zhai, C., Du, N., Zhang, H., Yu, J., Wu, P., Xiao, C., Assembling $CoSn_3$ nanoparticles on multiwalled carbon nanotubes with enhanced lithium storage properties. *Nanoscale*, 2011, 3, 1798.

[18] Yan, J., Song, H., Yang, S., Yan, J., Chen, X. Preparation and electrochemical properties of composites of carbon nanotubes loaded with Ag and TiO_2 nanoparticle for use as anode material in lithium-ion batteries. *Electrochimica Acta*, 2008, 53, 6351.

[19] Fu, Y., Ma, R., Shu, Y., Cao, Z., Ma, X. Preparation and characterization of SnO_2/carbon nanotube composite for lithium ion battery applications. *Material Letters*, 2009, 63, 1946.

[20] Tocoglu, U., Alaf, M., Cevher, O., Guler, M.O., Akbulut, H., The effect of oxidants on the formation of multi-walled carbon nanotube buckypaper. *Journal of Nanoscience and Nanotechnology*, 2012, 12, 9169.

[21] Teague, L.C., Banerjee, S., Wong, S.S., Richter, C.A., Varughese, B., Batteas, J.D. Effects of ozonolysis and subsequent growth of quantum dots on the electrical properties of freestanding single-walled carbon nanotube films. *Chemistry Physics Letters*, 2007, 442, 354.

[22] Gong, T., Zhang, Y., Liu, W.J., Wei, J.Q., Li, C.G., Wang, K.L. Connection of macro-sized double-walled carbon nanotube strands by bandaging with double-walled carbon nanotube films. *Carbon*, 2007, 45, 2235.

[23] Che, G., Lakshmi, B.B., Fisher, E.R., Martin, C.R. Carbon nanotubule membranes for electrochemical energy storage and production. *Nature*, 1998, 393, 346.

[24] Alaf, M., Gultekin, D., Akbulut, H., Electrochemical properties of free-standing Sn/SnO_2/multi-walled carbon nano tube anode papers for Li-ion batteries. *Applied Surface Science*, 2013, 275, 244.

[25] Thomas, R., Rao, K.Y., Rao, G.M., Morphology and electrochemical performance of graphene nanosheet array for Li-ion thin film battery, *Electrochimica Acta*, 2013, 108, 458..

[26] He, M., Yuan, L., Hu, X., Zhang, W., Shu, J., Huang, Y. A SnO_2@carbon nanocluster anode material with superior cyclability and rate capability for lithium-ion batteries. *Nanoscale*, 2013, 5, 3298.

[27] Zhao, Y., Li, J., Wang, N., Wu, C., Dong, G., Guan, L., Fully Reversible Conversion between SnO_2 and Sn in SWNTs@SnO_2@PPy Coaxial Nanocable As High Performance Anode Material for Lithium Ion Batteries. *Journal of Physical Chemistry C*, 2012, 116, 18612.